

Photoactive Excited States in Explosive Fe(II) Tetrazine Complexes: A Time-Dependent Density Functional Theory Study

Andrew E. Sifain,^{†,‡} Josiah A. Bjorgaard,^{‡,§} Thomas W. Myers,^{||} Jackie M. Veauthier,^{||} David E. Chavez,^{||} Oleg V. Prezhdo,^{†,⊥} R. Jason Scharff,^{*,#} and Sergei Tretiak^{*,‡,§,∇}

[†]Department of Physics and Astronomy, University of Southern California, Los Angeles, California 90089-0485, United States

[‡]Center for Nonlinear Studies, Los Alamos National Laboratory, Los Alamos, New Mexico 87545, United States

[§]Theoretical Division, Los Alamos National Laboratory, Los Alamos, New Mexico 87545, United States

^{||}Chemistry Division, Los Alamos National Laboratory, Los Alamos, New Mexico 87545, United States

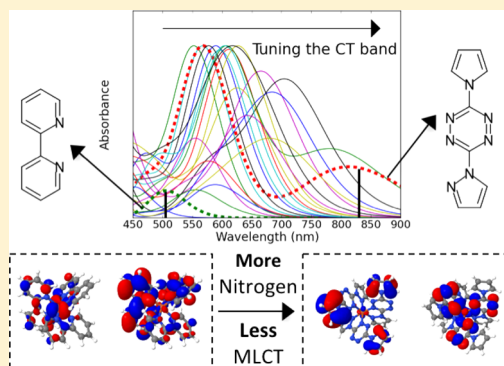
[⊥]Department of Chemistry, University of Southern California, Los Angeles, California 90089-1062, United States

[#]Explosives Science and Shock Physics Division, Los Alamos National Laboratory, Los Alamos, New Mexico 87545, United States

[∇]Center for Integrated Nanotechnologies, Los Alamos National Laboratory, Los Alamos, New Mexico 87545, United States

Supporting Information

ABSTRACT: Time-dependent density functional theory was used to investigate optical absorption of novel Fe(II) coordination complexes with tetrazine ligands. These octahedral compounds absorb near-infrared (NIR) light and can be applied as secondary explosives with low laser-initiation thresholds compared to pentaerythritol tetranitrate. Herein, numerous ligand architectures are studied to determine relationships between molecular structure and optical absorption in order to tune the low-energy charge transfer (CT) band. Geometrical structures and vertical excitation energies calculated with the TPSSH density functional and 6-311G basis set are in excellent agreement with experiment, with a maximum deviation from UV–vis spectra of 0.10 eV. By altering molecular substituents of the ligand scaffold, the CT band can be tuned between 500 and 1100 nm. Additional conjugation in the ligand scaffold pushes the CT band into the NIR region of the spectrum. Triazolo-tetrazine ligands shift the CT band by approximately 0.70 eV relative to that of Fe(II) coordinated with bipyridine ligands. Oxygenated analogues of several compounds are also studied in order to predict optical response, while improving explosive performance. A natural population analysis suggests that the high nitrogen content of the ligand scaffolds in these energetic compounds lessens their metal-to-ligand charge transfer character compared to that of Fe(II) coordinated with bipyridine ligands. The proposed model quantum chemistry is used to establish structure–property relationships for optical properties in this class of materials in order to make optical initiation with conventional lasers a more feasible approach.



INTRODUCTION

Coordination complexes have gained worldwide attention due to their rich photophysical properties. Fe(II) and Ru(II) polypyridines have been utilized for light-harvesting in dye-sensitized solar cells.^{1–12} Cyclometalated Ir(III) complexes have seen use in organic light-emitting diodes,^{13,14} light-emitting electrochemical cells,^{15–23} photocatalysis,^{13,17,24–27} and even biotechnology.^{28–31} Needless to say, coordination complexes have been introduced in a variety of applications. One major advantage is their synthetic flexibility, which makes tuning their photophysical properties possible. A new application utilizing coordination complexes is the design of photoactive explosives.

Current methods used to detonate high explosives rely on mechanical or electrical initiation and are susceptible to accidental initiation from mechanical or electrical insults.

Optical initiation is a promising alternative that offers enhanced safety.^{32,33} Replacing electrical components with fiber optics eliminates the susceptibility to electrical insult, while replacing sensitive primary explosives with less sensitive photoactive secondary explosives reduces the susceptibility to mechanical insult. In spite of these advantages, optical initiation systems have been limited by a lack of suitable photoactive explosives.³⁴ Sensitive primary explosives such as lead azide have low laser-initiation thresholds but are too dangerous to employ,³⁵ while less sensitive secondary explosives such as pentaerythritol tetranitrate (PETN), 1,3,5-trinitroperhydro-1,3,5-triazine (RDX), and octahydro-1,3,5,7-tetranitro-1,3,5,7-tetrazocine

Received: October 12, 2016

Revised: November 17, 2016

Published: November 29, 2016

(HMX) have laser-initiation thresholds that require too much energy to be of practical use.^{36,37} Primary explosives that are less sensitive than lead azide have been proposed, but with initiation thresholds in the near-infrared (NIR) at energy densities several orders of magnitude more than that of lead azide.^{38–41} Decreasing the density of PETN can reduce the laser-initiation threshold, but also renders the material more mechanically sensitive. Doping PETN with an optically absorbent material such as metal nanoparticles can further reduce the initiation threshold to a small degree, but does not address the safety concerns.

Recently reported Fe(II) coordination complexes with tetrazine ligands absorb NIR light.^{42,43} Tetrazines have rich spectroscopic properties both as organic compounds⁴⁴ and as ligands in coordination complexes.^{45,46} The number of C–N and N–N bonds in these ligands increases their heat of formation compared to those of conventional carbon-based molecules, thus making them more energetic.^{47–50} Their spectroscopic properties in combination with their low laser-initiation thresholds, mechanical sensitivity, and explosive performance make them viable laser-initiated secondary explosives.⁴² Recent works outline the syntheses and characterizations of many high explosive materials^{51,52} and, in particular, those of Fe(II) tetrazine complexes with metal-to-ligand charge transfer (MLCT) character.^{42,43,53,54} It is beneficial to further elucidate structure–property relationships characterizing the low-energy CT band from a theoretical perspective to enhance control over the initiation threshold.

Molecular structure influences absorption and can be altered to tailor-design energetic materials. A recent theoretical work has studied the effect of molecular structure on linear and nonlinear optical response in small, conjugated energetic molecules.⁵⁵ Herein, time-dependent density functional theory (TD-DFT)⁵⁶ is used to study linear absorption in Fe(II) complexes with different ligand architectures. TD-DFT generally offers an accurate description of the excited-state electronic structure of large molecular systems.^{57,58} Due to the availability of high power Nd:YAG lasers, the most practical wavelength for initiation is 1064 nm. By studying how these architectures affect absorption, one can uncover design principles, leading to a class of explosives with the desired optical response. Most importantly, tuning the low-energy CT band is relevant to many technological applications that utilize the optical properties of octahedral transition-metal complexes.

METHODS

Computational. Absorption spectra were calculated with various levels of theory and compared to experimental data. A detailed comparison of these methods is presented and discussed in the following section. Overall, the TPSSh density functional⁵⁹ and 6-311G basis set⁶⁰ showed the best performance. We have chosen this combination to optimize ground-state geometries and calculate vertical excitation energies for all molecules in this study. No symmetry constraints were imposed on optimization. Each vertical excitation was represented as a broadened Gaussian with a standard deviation of 0.15 eV. A total of 70 singlet excited states were requested in the TD-DFT calculation and used to compute each spectrum. All quantum-chemical calculations were obtained with the Gaussian 09 software package.⁶¹ The polarizable continuum model (PCM)⁶² was used in the linear response formalism^{63–65} to simulate the dielectric effects of an acetone (dielectric constant, $\epsilon = 20.493$) solvent environment.

The TPSS functional⁶⁶ stems from the meta-generalized gradient approximation (MGGA) and requires finite exchange potential, thereby eliminating erroneous effects of ground-state one- and two-electron orbital densities, which are ubiquitous due to the hydrogen atom and chemical bond. The TPSS hybrid⁵⁹ (TPSSh) incorporates 10% Hartree–Fock exchange and satisfies the same exact constraints as TPSS. TPSSh surpasses the best available semiempirical methods and is a more uniformly accurate description of diverse systems and properties.⁵⁹ Past works with the TPSSh functional show that it accurately describes equilibrium geometries in first-⁶⁷ and second-row⁶⁸ transition-metal complexes, binding energies in transition-metal diatomics⁶⁹ and dimers,⁷⁰ and ligand dissociation energies of large cationic transition-metal complexes.⁷¹

Natural transition orbital (NTO) analysis of the dominant electronic transitions within the low-energy charge transfer (CT) band was performed. NTOs offer the most compact, qualitative representation of the specified transition density expanded in terms of single-particle transitions.^{64,72} Therefore, NTOs offer a simple way of assigning the transition character. NTOs were calculated with the TPSSh functional and 6-311G basis set. Figures showing NTOs were obtained with the Jmol program.⁶⁵

A natural population analysis^{73,74} (NPA) was performed to calculate MLCT character. The NPA used the configuration interaction singles (CIS) excited- and ground-state densities in the natural atomic orbital (NAO) basis using NBO 3.1.⁷⁵ The difference in charge was then used as an MLCT indicator. The spatial diffuseness of the NAO basis set is optimized for calculating the effective atomic charge and can, therefore, be used to calculate local charge shifts that would otherwise require variational contributions from multiple basis functions of variable range such as double- ζ , triple- ζ , etc. The B3LYP density functional⁷⁶ was used to compute these charges due to the limited functionality of TPSSh in the Gaussian 09 software package. The B3LYP and 6-311G combination, however, is in good agreement with UV–vis, and several spectra are available in the following section.

Experimental. Atomic coordinates for several of the compounds were obtained from their previously reported solid-state structures using X-ray diffraction experiments.⁴² Absorption spectra were recorded with an HP 8453 Agilent UV–vis spectrometer. Materials were dissolved in solutions of acetone at concentrations of 2×10^{-4} M. All spectra, both experimental and theoretical, were normalized by the magnitude of maximum absorption to convey relative intensity.

RESULTS AND DISCUSSION

The results are organized as follows: First, we systematically choose a model quantum chemistry, which is validated with experimental solid-state structures and absorption spectra for several compounds. Second, we apply the theory to calculate the absorption spectra in a series of compounds with various ligand architectures to determine structure–property relationships that tune the low-energy CT band. Third, we do the same analysis as that done in the preceding section, but with oxygenated analogues of several of the compounds. Lastly, we characterize the CT bands of these compounds by explicitly calculating MLCT character.

Benchmarking Model Quantum Chemistry. In order to utilize an appropriate model quantum chemistry for this study, theoretical calculations using different levels of theory were compared to the experimental data of several recently

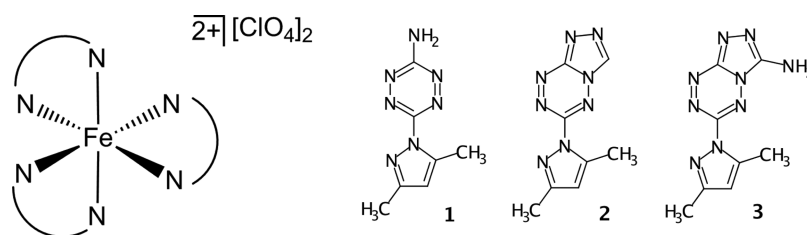


Figure 1. Octahedral geometry and ligands of Fe(II) complexes 1–3.

synthesized compounds. The group of octahedral compounds and their associated ligands are shown in Figure 1. Previous TD-DFT representative simulations using the B3LYP functional and 6-31G* basis set^{77,78} have shown very limited predictive accuracy, which warrants a more detailed computational investigation of this family of molecules.⁴² In experiments, perchlorate counterions were utilized to improve the oxygen balance in the resulting complexes. Ligands 1–3 react with $[\text{Fe}(\text{H}_2\text{O})_6][\text{ClO}_4]_2$ in MeCN to form $[(\text{NH}_2\text{TzDMP})_3\text{Fe}][\text{ClO}_4]_2$, $[(\text{TriTzDMP})_3\text{Fe}][\text{ClO}_4]_2$, and $[(\text{NH}_2\text{-TriTzDMP})_3\text{Fe}][\text{ClO}_4]_2$, respectively. Since these counterions do not play a significant role in optical absorption, they were not incorporated into our simulations.

Single-crystal X-ray crystallography confirmed the geometries of complexes 1–3 as distorted octahedra with three tetrazine ligands. Shown in Table 1, the TPSSh and 6-311G combination

Table 1. Measured and Calculated Bond Lengths (Å) of Complexes 1–3. X-ray Diffraction Measurements Are in Parentheses

complex	Fe–N _{Tz}	Fe–N _{pyr}	N _{Tz} –N _{Tz}
1	1.896 (1.907(6))	1.982 (1.953(6))	1.339 (1.318(4)), 1.343 (1.318(4))
2	1.899 (1.911(3))	1.980 (1.980(3))	1.323 (1.307(3)), 1.371 (1.358(3))
3	1.902 (1.894(5))	1.974 (1.959(5))	1.333 (1.311(5)), 1.383 (1.358(5))

calculates bond lengths within 0.03 Å of measured values. The most notable feature is the effect of the 1,2,4-triazolo[4,3-*b*]-[1,2,4,5]-tetrazine fused ring system on the N_{Tz}–N_{Tz} bonds of 2 and 3. As opposed to 1, where N_{Tz}–N_{Tz} are of similar length, 2 and 3 have N_{Tz}–N_{Tz} bonds of different lengths; the larger of the two is located farther away from the Fe atom. This is due to the loss of double bond delocalization imposed by the fused ring system.⁴²

Figure 2 shows TD-DFT results computed with four different methods. The TPSSh and 6-311G method (shown in blue) accurately describes many important features of the absorption spectra. The location of the low-energy CT band matches exceptionally well with experiment for all three compounds and are recovered to within 0.10 eV. The CT band shifts to higher wavelengths from 1 to 3 in numerical order, thereby showing how the triazolo-tetrazine fused ring system tunes the CT band to lower energies. Other observations that validate the use of the proposed method are the high-energy peaks, which are mainly π – π^* excitations localized on the ligands. In 1, three peaks ranging from 300 to 500 nm are recovered in nearly the exact locations. The peaks in 2 and 3 are also recovered, but are slightly red-shifted compared to experiment.

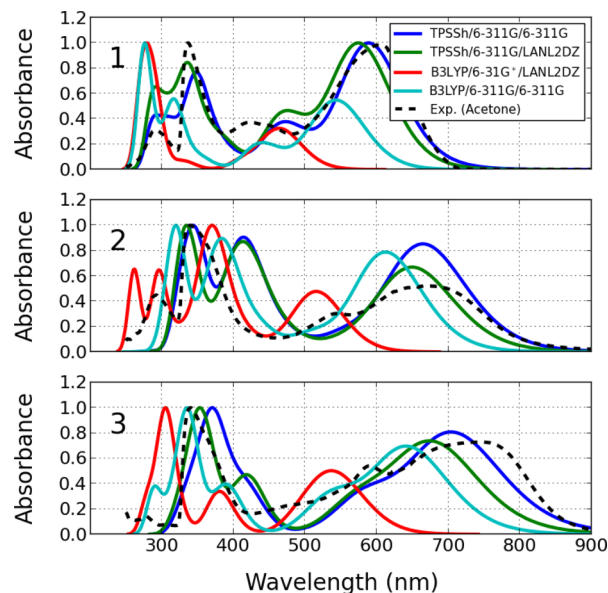


Figure 2. Optical absorption of complexes 1–3 computed with different levels of theory. The indices from left to right refer to functional, basis set on nonmetal atoms, and basis set on the Fe atom. UV–vis spectra in acetone are shown with dashed lines.

Several studies of transition-metal complexes have utilized the relativistic effective core potential (RECP), LANL2, and its associated basis set, LANL2DZ, on the metal atom.^{27,79–81} The RECP replaces inner core electrons, while leaving explicit treatment of outer electrons.^{82,83} On the basis of our findings in Figure 2, however, LANL2DZ (shown in green) is slightly inferior to 6-311G on all atoms since the CT band is blue-shifted compared to experiment for all three compounds. LANL08 is an uncontracted version of LANL2DZ, giving the basis set more flexibility to adjust to the DFT potential.^{84–86} Performance of LANL08 is shown in Figure S1 of the Supporting Information. Given these results, we did not choose a pseudo description of the Fe atom via LANL2DZ or LANL08.

The B3LYP functional with the 6-31G* basis set on nonmetal atoms and LANL2DZ on the Fe atom was the method of choice in a previous study (shown in red).⁴² It is clearly the worst performing method in Figure 2, especially at low energies. The low-energy CT bands are severely blue-shifted from UV–vis from about 0.50 eV in 1 to 0.70 eV in 3. Also, the relative intensities of the CT bands are noticeably reduced compared to those observed experimentally and those which are predicted with the TPSSh functional. Results using the B3LYP functional are significantly improved with the 6-311G basis set on all atoms (shown in cyan). Deviation from UV–vis is reduced to about 0.20 eV in 1 to 0.25 eV in 3. Overall, the B3LYP and 6-311G combination is in good

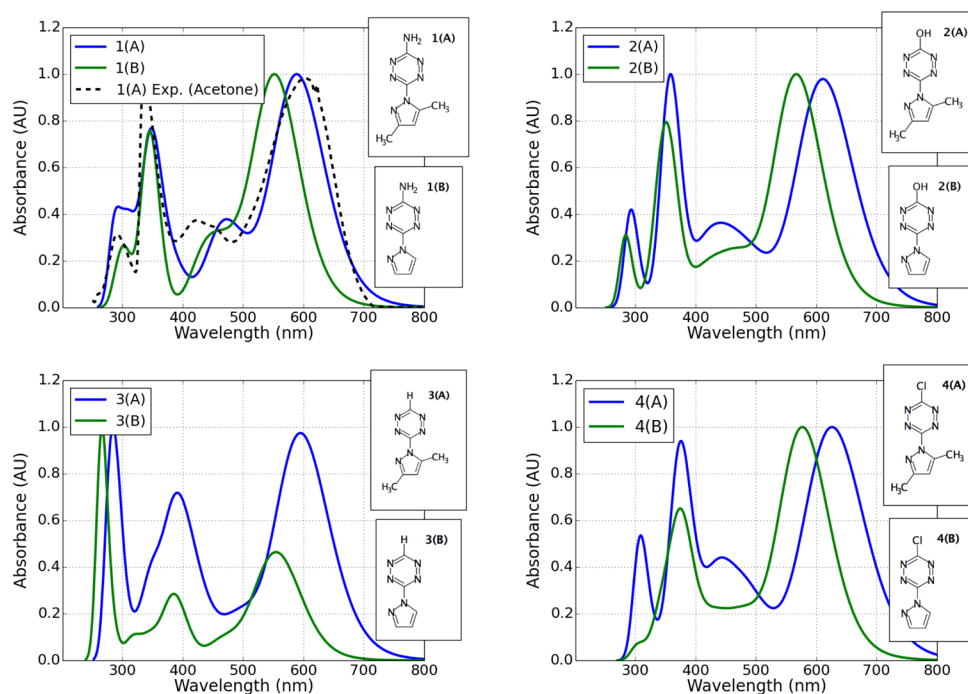


Figure 3. Optical absorption of complexes 1–4. The ligands for each associated octahedral complex are shown. The UV–vis spectrum of 1(A) in acetone is shown with a dashed line.

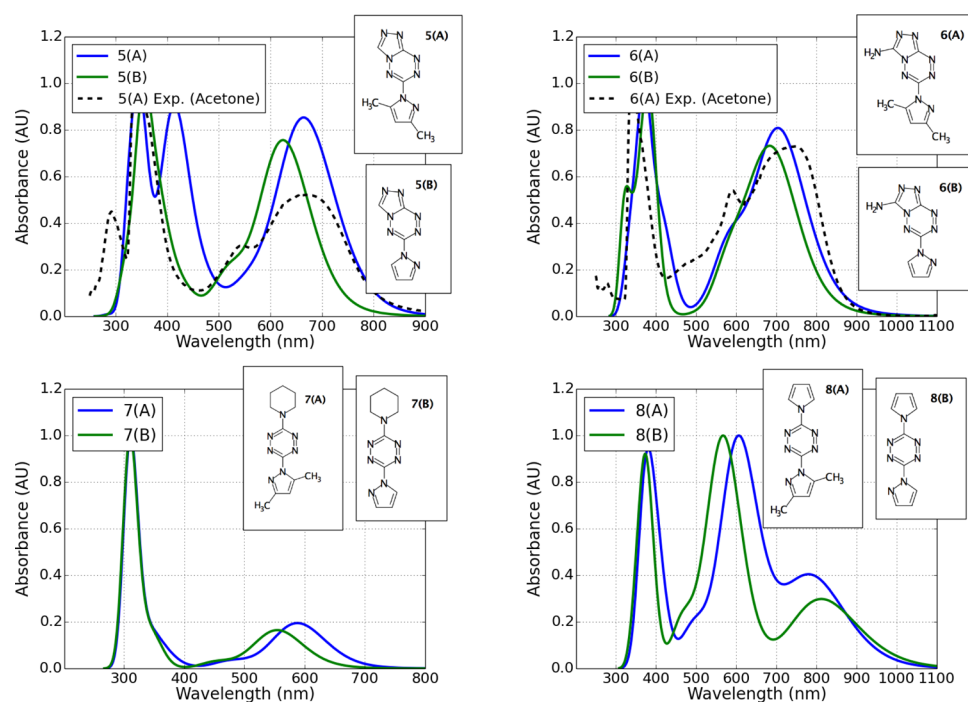


Figure 4. Optical absorption of complexes 5–8. The ligands for each associated octahedral complex are shown. UV–vis spectra of 5(A) and 6(A) in acetone are shown with dashed lines.

qualitative agreement with UV–vis spectra. We have chosen this method to calculate natural populations in an upcoming section. Again, this is due to the limited functionality of the TPSSH functional in the Gaussian 09 software package.

The effects of adding polarization functions to the basis sets were analyzed. Results are shown in Figure S2 of the Supporting Information. Polarization on the Fe atom did not affect absorption, while polarization on nonmetal atoms blue-shifted the spectra by less than 0.2 eV compared to UV–vis,

which is still within reasonable accuracy for TD-DFT. We have chosen not to add polarization in our final choice of basis set since the spectra for our three test compounds were not improved. An extension to larger basis sets does not necessarily improve the results in large conjugated molecules,⁸⁷ since optical response originates from mobile π -electrons that are strongly delocalized. Hence, the contribution of atomic polarization is minimal.

Optical Absorption of Explosive Compounds. We applied TD-DFT to predict the optical absorption in several compounds. The first group of ligands and absorption spectra of the associated complexes are shown in Figure 3. In order to explore the influence of chemical structure on absorption, the substituents bound to position 3 of the tetrazine system were varied: NH₂ (1), OH (2), H (3), and Cl (4). Compound 1 of Figure 1 is labeled as 1(A) in Figure 3.

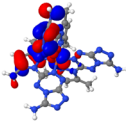
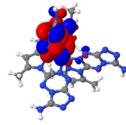
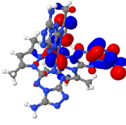
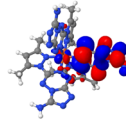
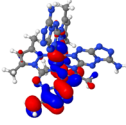
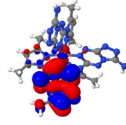
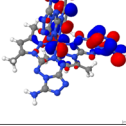
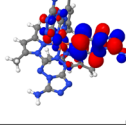
To reduce carbon content, a pyrazole counterpart was included in the study. Dimethylpyrazole- and pyrazole-containing ligands are labeled by A and B, respectively. The pyrazole systems increase oxygen balance and are useful for optical initiation. The low-energy CT bands of the pyrazole compounds are blue-shifted relative to those of the dimethylpyrazole compounds. The peak location of their CT bands varies between 555 nm in 1(B), 555 nm in 3(B), 570 nm in 2(B), and 580 nm in 4(B). In the dimethylpyrazole compounds, it varies between 590 nm in 1(A), 595 nm in 3(A), 610 nm in 2(A), and 630 nm in 4(A). The additional oxygen in 2 further increases oxygen balance, which may improve its explosive performance. On the basis of Figure 3, the CT band can be tuned between approximately 500 and 800 nm within this group of ligand architectures. It would be beneficial to further shift the CT band toward lower energies since optical initiation with NIR lasers is the optimal choice for practical purposes.

To determine the effect of molecular size and conjugation of the ligand scaffold on absorption, a second group of compounds were studied. The ligands and absorption spectra of the associated complexes are shown in Figure 4. These compounds are composed of more atoms than those shown in Figure 3. Compounds 2 and 3 of Figure 2 are labeled as 5(A) and 6(A) in Figure 4, respectively. The piperidine and pyrrole systems, bound to position 3 of the tetrazine systems, are labeled as 7 and 8, respectively.

Figure 4 also shows the low-energy CT bands of the pyrazole compounds blue-shifted relative to those of the dimethylpyrazole compounds. The peak location of their CT bands varies between 555 nm in 7(B), 625 nm in 5(B), 690 nm in 6(B), and 830 nm in 8(B). In the dimethylpyrazole compounds, it varies between 590 nm in 7(A), 665 nm in 5(A), 710 nm in 6(A), and 800 nm in 8(A). Unlike the other compounds, there is an additional low-energy CT band appearing in 8(A) and 8(B), which will be analyzed in detail. On the basis of Figure 4, the CT band can be tuned between approximately 500 and 1100 nm within this group of ligand architectures. Overall, these compounds are more suitable for optical initiation with NIR light.

The triazolo-tetrazine fused ring system shown in 5 and 6 is a relatively large conjugated system compared to all other compounds in this data set. This suggests that conjugation in the ligand scaffold is an important design principle toward pushing the low-energy CT band into the NIR. The UV-vis spectrum of 5(A) diminishes slightly past 900 nm, whereas, for 6(A), with NH₂ bound to position 5 of the triazole, absorption diminishes slightly past 1000 nm. Therefore, functional groups, such as NH₂, further shift the CT band toward lower energy. It is worth exploring additional substituents in 6(A) to increase absorption at 1064 nm. The NTOs of 6(A), shown in Table 2, show predominantly partial MLCT and partial intraligand CT. The CT character is from the Fe core and NH₂ group to the tetrazine system for all electron-hole pairs. The NTOs of 5(A)

Table 2. NTOs of the Photoactive Excited States within the Low-Energy CT Band of 6(A). The Percent Contribution That Each Electron-Hole Pair Carries Toward the Transition Is Shown^a

λ (nm)	percent	hole	electron
708	55		
	43		
707	65		
	24		

^aNTOs displayed amount to at least 90% of the total transition.

show similar excitation character and are available in Table S1 of the Supporting Information.

Conformations of the ligand scaffolds in 5 and 6 were analyzed. There is a rotational degree of freedom between the tetrazine ring and both, the dimethylpyrazole systems of 5(A) and 6(A) and the pyrazole systems of 5(B) and 6(B). It is energetically favorable for the triazole ring to be further away from the Fe core. The molecular energy difference in the Hartree-Fock approximation between this geometry and the alternative geometry, in which the triazole is pointed toward the Fe core, is on the order of 100 times $k_B T$ at room temperature. Therefore, the orientation of the ligand scaffolds shown in Figure 4 is correct to within a high degree of certainty.

Similar to the triazolo-tetrazine fused ring systems of 5 and 6, spectral differences in 7 and 8 also stress the importance of conjugation in the ligand scaffold toward pushing the low-energy CT band into the NIR. Compounds 7(A) and 7(B), with piperidine systems bound to positions 3 of the tetrazine systems, have CT bands comparable to those of Figure 3, peaking at 555 and 590 nm, respectively. TD-DFT predicts an additional low-energy peak in 8(A) and 8(B), however, at 800 and 830 nm, respectively, with absorption diminishing slightly past 1100 nm. The peaks in 8(A) and 8(B) that are located at 610 and 575 nm, respectively, have very little MLCT character. These excitations are predominantly localized on the ligand scaffolds, and the associated NTOs are available in Table S1 of the Supporting Information. This may imply that the lowest-energy excitations in 8(A) and 8(B) are also not of MLCT character. We will verify this in a subsequent section. For now,

it is clear that the pyrrole system in **8** increases conjugation, which lowers optical excitation compared to that of the piperidine system in **7**. Compounds with the farthest red-shifted CT bands, and that are most suitable for optical initiation in the NIR, are **5**, **6**, and **8**.

Determining physical descriptors of the ligand scaffold that correlate to the location of the low-energy CT band is beneficial, as it may aid in the design of materials with a specific optical response. A recent study of Fe(II) coordination complexes, for example, shows how ligand field strength can be tuned by ligand design, influencing molecular and electronic structure.⁸⁸ It is generally true that charge distribution of the ground-state geometry affects electronic structure and the nature of electronic transitions. We calculate the quadrupole moments of the ligand scaffolds shown in Figures 3 and 4 using⁸⁹

$$Q_2^2 = \frac{4\pi}{5} \sum_m |Q_{2m}|^2 \quad (1)$$

where Q_{2m} are elements of the quadrupole moment in spherical coordinates. The azimuthal dependence is given by $m \in \{-2, -1, 0, 1, 2\}$. Results are shown in Figure 5.

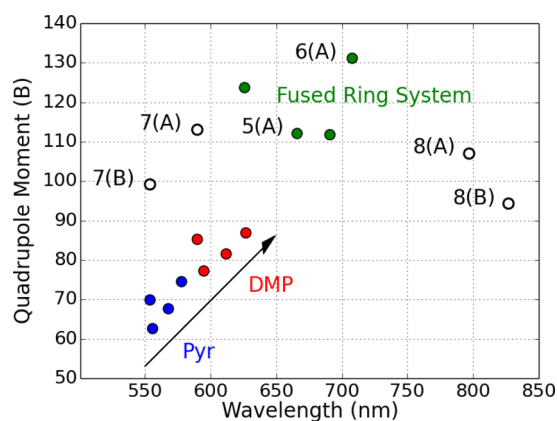


Figure 5. Quadrupole moment of the ligand scaffold in the ground-state geometry versus wavelength of the strongest photoactive excited state within the low-energy CT band. Pyr and DMP stand for pyrazole and dimethylpyrazole, respectively.

The pyrazole ligands, **1(B)**, **2(B)**, **3(B)**, and **4(B)**, with a single functional group bound to position 3 of the tetrazine system, are labeled by blue markers. The same ligands with dimethylpyrazole, **1(A)**, **2(A)**, **3(A)**, and **4(A)**, are shown in red. The quadrupole moment of the ligand scaffold correlates to the location of the low-energy CT band in these compounds. The wavelength shifts from 550–600 nm in the pyrazole compounds to 600–650 nm in the dimethylpyrazole compounds, with quadrupole moment increasing from 60–75 to 75–90 B, respectively. The same trend is observed with the triazolo-tetrazine compounds, which are labeled by green markers. The correlation is more dispersive than that of compounds **1–4**. The wavelength spans a range of approximately 630–710 nm with quadrupole moment increasing from 110 to 130 B, respectively. Figure 5 shows how the peak of the CT band can be tuned from approximately 550 to 710 nm between compounds **1–6** and that it roughly correlates to the quadrupole moment of the ligand scaffold.

Compounds **7** and **8** do not follow the same general trend as the remaining compounds of Figures 3 and 4. The pyrazole-

containing compound, **7(B)**, is blue-shifted compared to its dimethylpyrazole counterpart, **7(A)**, but the locations of their low-energy CT bands are similar to those of **1–4**. The large increase in quadrupole moment is likely correlated to its molecular size. Compound **8** has the lowest-energy CT band, exceeding 800 nm. As stated previously, **8** is unique from all other compounds since TD-DFT predicts an additional low-energy peak, not observed in the other compounds. It is an outlier, and we will show that the excitation character within this CT band is fundamentally different than all other compounds in this data set.

Tetrazines are readily derivatized with a variety of explosive groups. One such group is 3,3-dinitroazetidine (DNAZ), which can be attached to position 3 of the tetrazine system and is henceforth labeled as ligand **10(A)**. Ligand **10(A)** reacts with $[\text{Fe}(\text{H}_2\text{O})_6][\text{ClO}_4]_2$ in MeCN to form $[(\text{DNAZTzDMP})_3\text{Fe}][\text{ClO}_4]_2$. The ligand and absorption spectrum of the associated complex are shown in Figure 6. The TD-DFT calculations are

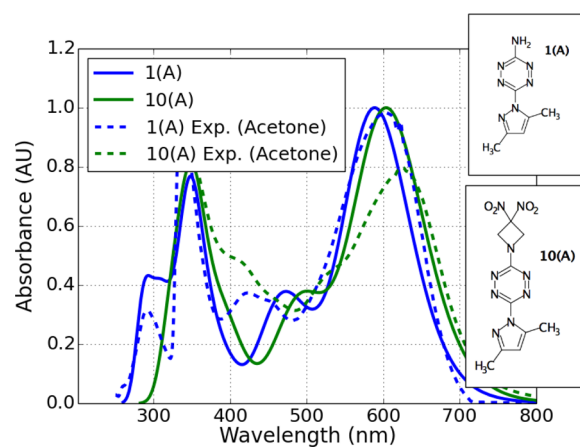


Figure 6. Comparison of the optical absorption in complexes **1(A)** and **10(A)**. The ligands of each associated octahedral complex are shown. UV–vis spectra of **1(A)** and **10(A)** in acetone are shown with dashed lines.

in excellent agreement with the UV–vis spectrum of **10(A)**, especially with the location of its low-energy CT band between 500 and 700 nm. The high-energy peak, located at approximately 350 nm, is also recovered in nearly the exact location. The calculations for **10(A)** required 150 excited states to obtain the visible region of the spectrum, as opposed to only 70 states for the remaining compounds, due to its large density of states. Compound **1(A)** is also shown in Figure 6 for comparison. The CT bands of **1(A)** and **10(A)** are very similar both in position and in magnitude, which are attributed to the fact that the NO_2 substituents of **10(A)** are far removed from the tetrazine system. The optical properties are largely dictated by the excitation character of the Fe core and tetrazine systems, and substituents that are within close proximity. This is validated by the NTOs of the low-energy transitions in **10(A)**, which show no charge distribution on the DNAZ system. These NTOs are available in Table S1 of the Supporting Information. Although the CT bands of **1(A)** and **10(A)** peak in similar locations, i.e., 590 and 605 nm, respectively, oxygenated ligands are important for explosive applications.

Oxygen-Containing Compounds. To increase oxygen balance and explosive performance, a set of compounds with oxygen substituents were studied. Ligands and absorption

spectra are shown in Figure 7. These compounds are labeled with C to denote that they are oxygenated analogues of their B

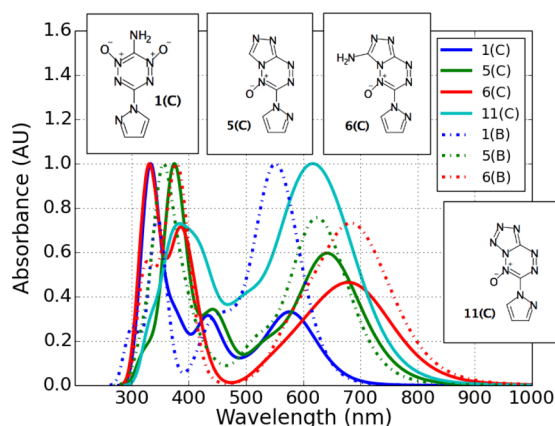


Figure 7. Optical absorption of complexes 1(C), 5(C), 6(C), and 11(C) with oxygen substituents. The absorption of 1(B), 5(B), and 6(B) without oxygen substituents is shown for comparison.

counterparts. For example, 1(C) is an oxygenated analogue of 1(B), where two oxygen substituents are bound to positions 2 and 4 of the tetrazine system. Compounds 5(C) and 6(C) are analogues of 5(B) and 6(B), respectively, where a single oxygen substituent is bound to position 1 of the tetrazine system. Lastly, 11(C) replaces the triazole with a tetrazole—a carbon atom is exchanged for a nitrogen—and a single oxygen substituent is bound to position 1 of the tetrazine system.

There are minor spectral differences between the non-oxygenated and oxygenated compounds. The peak location of the low-energy CT band in the oxygenated compounds varies between 580 nm in 1(C), 645 nm in 5(C), and 700 nm in 6(C). In the nonoxygenated compounds, it varies between 555 nm in 1(B), 625 nm in 5(B), and 690 nm in 6(B). Therefore, the CT band is slightly red-shifted in the oxygenated compounds relative to that of the nonoxygenated compounds. The absorption magnitude is predicted to be larger in the nonoxygenated compounds, however. The peak in 1(B) is over 3 times larger than that of 1(C). The same is true for 5(B) and 6(B) relative to 5(C) and 6(C), respectively, but with noticeably smaller differences. This is likely due to molecular size. Unlike 5 and 6, which are relatively large due to the fused ring system, 1 is smaller and, therefore, two oxygen substituents constitute a much larger fraction of the ligand scaffold, greatly affecting its electronegativity and electronic structure. It makes sense to compare 11(C) to 5(C) since they differ by only one atom. The peak location of the CT band in 11(C) is at 630 nm, as opposed to 645 nm in 5(C). Also, the absorption magnitude in 11(C) is predicted to be nearly twice that of 5(C). Similar to the findings in previous sections, 5(C), 6(C), and 11(C) enhance conjugation due to a fused ring system, and as a result, their CT bands are red-shifted compared to that of 1(C). Although the syntheses of compounds 5(C) and 6(C) have not yet been reported, these results qualitatively show that additional oxygen can increase their oxygen balance, while leaving their low-energy absorptions more or less unaffected.

Oxygen balance (OB%) provides a measure to which a material can be oxidized. Generally, optimal explosive performance is achieved as OB% approaches zero.⁹⁰ The following equation was used to compute OB%

$$\text{OB}\% = -\frac{1600}{M} \left(2X + \frac{1}{2}Y - Z \right) \quad (2)$$

where X, Y, and Z, are the number of carbon, hydrogen, and oxygen atoms, respectively, and M is the molecular weight of the compound. Perchlorate counterions were included in the calculation. Tabulated quantities are shown in Table 3. Most

Table 3. OB% of Several Compounds with and without Oxygen Substituents in Their Ligand Scaffolds

complex	OB%	λ (nm)
1(A)	−91.7	590
10(A)	−74.2	605
1(B)	−63.4	555
2(B)	−53.5	570
5(B)	−66.4	625
6(B)	−65.7	690
1(C)	−44.8	580
5(C)	−57.2	645
6(C)	−57.0	700
11(C)	−43.2	630

notable differences in OB% are between the base compounds and their oxygenated analogues such as 1(A) → 10(A), 1(B) → 2(B), 1(B) → 1(C), 5(B) → 5(C), and 6(B) → 6(C). Even a single oxygen substituent significantly increases the oxygen balance, which has strong implication on explosive performance. For example, the OB% increases from −66.4% and −65.7% in 5(B) and 6(B) to −57.2% and −57.0% in 5(C) and 6(C), respectively. Furthermore, the OB% increases from −57.2% to −43.2% with exchange of the triazole in 5(C) for a tetrazole in 11(C). Also noteworthy is the difference in OB% between the dimethylpyrazole-containing compound, 1(A), and its pyrazole counterpart, 1(B), where OB% increases from −91.7% to −63.4%, respectively. Again, these calculations support the claim that additional oxygen in the ligand scaffold significantly increases OB%, while preserving low-energy absorption.

Characterizing MLCT Bands. Transition-metal complexes are generally characterized as having strong MLCT character. It would be beneficial to compare the excitation character of these energetic compounds to a control group for classification. Two compounds with strong MLCT character are [Ru(bpy)₃]²⁺ and [Fe(bpy)₃]²⁺. We quantify the amount of CT from the metal core to the ligand scaffold by taking the difference of natural charge between the ground state and strongest photoactive excited states within the low-energy peaks. Results are shown in Figure 8. It is worth mentioning that the B3LYP functional and 6-311G basis set are used in the following analysis and that the absorption spectra using this method are usually blue-shifted compared to experiment, as evidenced in Figure 2. Nevertheless, the main goal is to obtain a qualitative comparison of the MLCT character.

There is a clear distinction between these energetic compounds and [Ru(bpy)₃]²⁺ and [Fe(bpy)₃]²⁺. Figure 8 shows [Ru(bpy)₃]²⁺ having the most MLCT character between 0.30 and 0.35 electrons. Its MLCT band falls within 400 and 500 nm, peaking at about 450 nm. This is in excellent agreement with experiment, where the MLCT band is reported to peak at 452 ± 3 nm.⁹¹ [Fe(bpy)₃]²⁺ has less MLCT character than [Ru(bpy)₃]²⁺, with MLCT between 0.20 and 0.25 electrons. The MLCT band of [Fe(bpy)₃]²⁺ is slightly red-

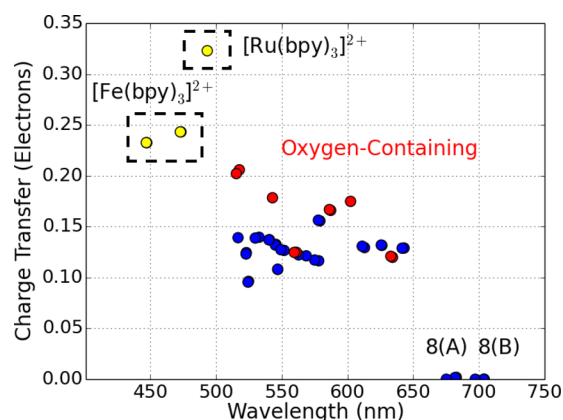


Figure 8. MLCT, in units of number of electrons, versus wavelength of the strongest photoactive excited states within the low-energy CT band.

shifted compared to $[\text{Ru}(\text{bpy})_3]^{2+}$, which also agrees with experiment.⁹² The majority of compounds, which are labeled by red and blue markers, fall within an MLCT of 0.10 and 0.20 electrons and with low-energy CT bands peaking between 500 and 650 nm. The ligand scaffolds of these energetic compounds have a higher nitrogen content than the bipyridine ligands of $[\text{Ru}(\text{bpy})_3]^{2+}$ and $[\text{Fe}(\text{bpy})_3]^{2+}$. Therefore, these results suggest that the CT band in complexes with more nitrogen-rich and electron-poor ligands occur at lower energies and with less MLCT character.

The reason these energetic compounds have less MLCT character than $[\text{Ru}(\text{bpy})_3]^{2+}$ and $[\text{Fe}(\text{bpy})_3]^{2+}$ is indeed attributed to their high nitrogen content. A higher nitrogen content of the ligand scaffold increases electronegativity, which means more charge will be displaced from the metal core to the ligand scaffold in the ground state. Therefore, during a transition into an excited state, there will be less MLCT. A prime example of this can be seen between compounds **1(B)** of Figure 3 and **1(C)** of Figure 7. The ligand scaffolds of **1(C)** have two additional oxygen substituents not present in **1(B)**, making **1(C)** more electron-rich. As a result, there will be more MLCT in the excitations of **1(C)** compared to those of **1(B)**. We calculate approximately 0.14 and 0.21 electrons in **1(B)** and **1(C)**, respectively. From a visual perspective, the NTOs of **1(C)** in Table 4 qualitatively show more MLCT character than **1(B)**. On the other hand, compounds **1(A)** and **10(A)** have similar MLCT character with 0.13 electrons. Again, the excitation character in these compounds is similar since the additional substituents in **10(A)** are far removed from the tetrazine system, which withholds most control over the optical properties.

Compounds **8(A)** and **8(B)** have very different excitation character than all other compounds shown in Figure 8. Their lowest-energy CT bands peak at approximately 700 nm using B3LYP and 6-311G, with little to no MLCT character. The NTOs of **8(B)**, obtained with TPSSh and 6-311G, are shown in Table 5. There is significant CT from the pyrrole to the tetrazine system for all electron–hole pairs. The CT character on the Fe atom is minimal. Compound **8** has the lowest-energy CT band and the largest amount of intraligand CT character among all other compounds, suggesting that additional conjugation in the ligand scaffold via the pyrrole system influences this type of excitation and is an important design principle that shifts the CT band toward lower energies.

Table 4. NTOs of Photoactive Excited States within the Low-Energy CT Bands of **1(B)** and **1(C)**. The Percent Contribution That Each Electron–Hole Pair Carries Toward the Transition Is Shown^a

complex	λ (nm)	percent	hole	electron
1(B)	554	63		
		28		
1(C)	580	64		
		26		

^aNTOs displayed amount to at least 90% of the transition.

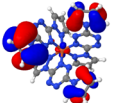
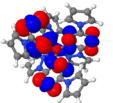
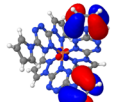

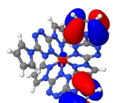

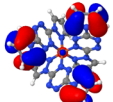

CONCLUSIONS

We utilized TD-DFT to study a class of transition-metal complexes. Past works support the use of MGGAs to describe bond lengths and dissociation energies. Their performance toward optically excited electronic states, however, warrants further investigation.⁹³ In this work, we have benchmarked the TPSSh functional against a series of novel and energetic Fe(II) coordination complexes. TD-DFT was found to be in excellent agreement with all UV–vis spectra with a maximum deviation of 0.10 eV. This gives us confidence in this model quantum chemistry toward predicting ways of lowering the initiation threshold.

We studied a large set of explosive compounds shown in Figures 3 and 4. The pyrazole-containing ligands shift the CT band toward lower energy, but their explosive performance is potentially weakened by additional carbon and hydrogen. In total, the CT band can be tuned between 500 and 1100 nm. Compounds with the lowest-energy CT bands and that are most suitable for optical initiation in the NIR are **5**, **6**, and **8**, which are due to additional conjugation in the ligand scaffold. This presents itself in **5** and **6** via the 1,2,4-triazolo[4,3-*b*]–[1,2,4,5]-tetrazine fused ring system, while, for **8**, it is the pyrrole system. In order to increase oxygen balance and improve explosive performance, a set of compounds with oxygen-containing ligands were also studied and are shown in Figure 7. In addition to the fused ring system, electron-donating groups, such as NH_2 , can further shift the CT band toward lower energy, as evidenced by **6(C)** in Figure 7.

We characterized the MLCT bands of these compounds by explicitly calculating effective charge on the metal core in the

Table 5. NTOs of Photoactive Excited States within the Low-Energy CT Band of 8(B). The Percent Contribution That Each Electron–Hole Pair Carries Toward the Transition Is Shown^a

λ (nm)	percent	hole	electron
831	90		
831	88		
	11		
823	91		

^aNTOs displayed amount to at least 90% of the transition.

ground and photoactive excited states. We found less MLCT character in these compounds than other commonly studied octahedral transition-metal complexes, such as $[\text{Fe}(\text{bpy})_3]^{2+}$ and $[\text{Ru}(\text{bpy})_3]^{2+}$. We attribute this to the high nitrogen content present in their ligand scaffolds. Compound 8, with pyrrole bound to position 3 of the tetrazine system, shows little to no MLCT, but rather mostly intraligand CT character. This suggests that increasing conjugation in the ligand scaffold lowers both excitation energies and MLCT.

To recapitulate, a theoretical study of the optical absorption in energetic Fe(II) coordination complexes has been accomplished. Vertical excitation energies computed with the TPSSh density functional and 6-311G basis set match exceptionally well with experiment. This supports the use of this nonempirical MGGA for optical absorption. The absorption spectra of these compounds strongly depend on the ligand scaffold and can be controlled by chemical substitution. Altering molecular substituents can push the CT band into the region of 1064 nm, which is a practical wavelength for optical initiation due to the availability of high power Nd:YAG lasers. The tetrazine-triazolo fused ring system shifts absorption to lower energies and is an important design principle. Compound 8 has not yet been synthesized, but is predicted to be within range for optical initiation. It is worth investigating additional conjugation in the ligand scaffold, such as fusing two triazolo rings to a central tetrazine. This study not only aids in the ongoing effort to design explosive materials that are both safer to handle and easier to initiate with NIR lasers than PETN but also is important for many light-harvesting

applications, where control over the photophysical properties is desirable.

■ ASSOCIATED CONTENT

Supporting Information

The Supporting Information is available free of charge on the ACS Publications website at DOI: 10.1021/acs.jpcc.6b10333.

Optical absorption of complexes 1–3 calculated with other density functionals and basis sets and compared to experiment. NTOs of 5(A), 8(B), and 10(A) (PDF)

■ AUTHOR INFORMATION

Corresponding Authors

*E-mail: scharff@lanl.gov (R.J.S.).

*E-mail: serg@lanl.gov (S.T.).

ORCID

Andrew E. Sifain: 0000-0002-2964-1923

Oleg V. Prezhdo: 0000-0002-5140-7500

Notes

The authors declare no competing financial interest.

■ ACKNOWLEDGMENTS

The authors acknowledge support of the U.S. Department of Energy through the Los Alamos National Laboratory (LANL) LDRD Program. LANL is operated by Los Alamos National Security, LLC, for the National Nuclear Security Administration of the U.S. Department of Energy under contract DE-AC52-06NA25396. This work was done in part at the Center for Nonlinear Studies (CNLS) and the Center for Integrated Nanotechnology (CINT) at LANL. We also acknowledge the LANL Institutional Computing (IC) program for providing computational resources. O.V.P. and A.E.S. acknowledge support of the US Department of Energy, Grant No. DE-SC0014429. A.E.S. thanks CNLS for their hospitality.

■ REFERENCES

- Jakubikova, E.; Bowman, D. N. Fe(II)-Polypyridines as Chromophores in Dye-Sensitized Solar Cells: A Computational Perspective. *Acc. Chem. Res.* **2015**, *48*, 1441–1449.
- Nazeeruddin, M. K.; De Angelis, F.; Fantacci, S.; Selloni, A.; Viscardi, G.; Liska, P.; Ito, S.; Takeru, B.; Grätzel, M. Combined Experimental and DFT-TDDFT Computational Study of Photoelectrochemical Cell Ruthenium Sensitizers. *J. Am. Chem. Soc.* **2005**, *127*, 16835–16847.
- Ardo, S.; Meyer, G. J. Photodriven Heterogeneous Charge Transfer with Transition-Metal Compounds Anchored to TiO₂ Semiconductor Surfaces. *Chem. Soc. Rev.* **2009**, *38*, 115–164.
- Nazeeruddin, M. K.; Pechy, P.; Grätzel, M. Efficient Panchromatic Sensitization of Nanocrystalline TiO₂ Films by a Black Dye Based on a Trithiocyanato-Ruthenium Complex. *Chem. Commun.* **1997**, 1705–1706.
- Ferrere, S. New Photosensitizers Based Upon $[\text{Fe}(\text{L})_2(\text{CN})_2]$ and $[\text{Fe}(\text{L})_3]$ (L = substituted 2, 2'-bipyridine): Yields for the Photosensitization of TiO₂ and Effects on the Band Selectivity. *Chem. Mater.* **2000**, *12*, 1083–1089.
- Ferrere, S. New Photosensitizers Based Upon $[\text{Fe}^{\text{II}}(\text{L})_2(\text{CN})_2]$ and $[\text{Fe}^{\text{II}}\text{L}_3]$, where L is Substituted 2, 2'-Bipyridine. *Inorg. Chim. Acta* **2002**, *329*, 79–92.
- Ferrere, S.; Gregg, B. A. Photosensitization of TiO₂ by $[\text{Fe}^{\text{II}}(2, 2'$ -bipyridine-4, 4'-dicarboxylic acid)₂(CN)₂]: Band Selective Electron Injection from Ultra-Short-Lived Excited States. *J. Am. Chem. Soc.* **1998**, *120*, 843–844.

- (8) Yang, M.; Thompson, D. W.; Meyer, G. J. Charge-Transfer Studies of Iron Cyano Compounds Bound to Nanocrystalline TiO₂ Surfaces. *Inorg. Chem.* **2002**, *41*, 1254–1262.
- (9) Yang, M.; Thompson, D. W.; Meyer, G. J. Dual Pathways for TiO₂ Sensitization by Na₂[Fe(bpy)(CN)₄]. *Inorg. Chem.* **2000**, *39*, 3738–3739.
- (10) Xia, H.-L.; Ardo, S.; Narducci Sarjeant, A. A.; Huang, S.; Meyer, G. J. Photodriven Spin Change of Fe (II) Benzimidazole Compounds Anchored to Nanocrystalline TiO₂ Thin Films. *Langmuir* **2009**, *25*, 13641–13652.
- (11) Monat, J. E.; McCusker, J. K. Femtosecond Excited-State Dynamics of an Iron (II) Polypyridyl Solar Cell Sensitizer Model. *J. Am. Chem. Soc.* **2000**, *122*, 4092–4097.
- (12) Huse, N.; Cho, H.; Hong, K.; Jamula, L.; de Groot, F. M.; Kim, T. K.; McCusker, J. K.; Schoenlein, R. W. Femtosecond Soft X-ray Spectroscopy of Solvated Transition-Metal Complexes: Deciphering the Interplay of Electronic and Structural Dynamics. *J. Phys. Chem. Lett.* **2011**, *2*, 880–884.
- (13) Ulbricht, C.; Beyer, B.; Friebe, C.; Winter, A.; Schubert, U. S. Recent Developments in the Application of Phosphorescent Iridium (III) Complex Systems. *Adv. Mater.* **2009**, *21*, 4418–4441.
- (14) Evans, R. C.; Douglas, P.; Winscom, C. J. Coordination Complexes Exhibiting Room-Temperature Phosphorescence: Evaluation of Their Suitability as Triplet Emitters in Organic Light Emitting Diodes. *Coord. Chem. Rev.* **2006**, *250*, 2093–2126.
- (15) Bolink, H. J.; Cappelli, L.; Coronado, E.; Grätzel, M.; Ortí, E.; Costa, R. D.; Viruela, P. M.; Nazeeruddin, M. K. Stable Single-Layer Light-Emitting Electrochemical Cell using 4, 7-Diphenyl-1, 10-phenanthroline-bis(2-phenylpyridine)iridium(III) Hexafluorophosphate. *J. Am. Chem. Soc.* **2006**, *128*, 14786–14787.
- (16) Su, H.-C.; Fang, F.-C.; Hwu, T.-Y.; Hsieh, H.-H.; Chen, H.-F.; Lee, G.-H.; Peng, S.-M.; Wong, K.-T.; Wu, C.-C. Highly Efficient Orange and Green Solid-State Light-Emitting Electrochemical Cells Based on Cationic Ir (III) Complexes with Enhanced Steric Hindrance. *Adv. Funct. Mater.* **2007**, *17*, 1019–1027.
- (17) Lowry, M. S.; Bernhard, S. Synthetically Tailored Excited States: Phosphorescent, Cyclometalated Iridium (III) Complexes and Their Applications. *Chem. - Eur. J.* **2006**, *12*, 7970–7977.
- (18) Parker, S. T.; Slinker, J. D.; Lowry, M. S.; Cox, M. P.; Bernhard, S.; Malliaras, G. G. Improved Turn-On Times of Iridium Electroluminescent Devices by Use of Ionic Liquids. *Chem. Mater.* **2005**, *17*, 3187–3190.
- (19) Bolink, H. J.; Cappelli, L.; Coronado, E.; Parham, A.; Stössel, P. Green Light-Emitting Solid-State Electrochemical Cell Obtained from a Homoleptic Iridium (III) Complex Containing Ionically Charged Ligands. *Chem. Mater.* **2006**, *18*, 2778–2780.
- (20) Nazeeruddin, M. K.; Wegh, R.; Zhou, Z.; Klein, C.; Wang, Q.; De Angelis, F.; Fantacci, S.; Grätzel, M. Efficient Green-Blue-Light-Emitting Cationic Iridium Complex for Light-Emitting Electrochemical Cells. *Inorg. Chem.* **2006**, *45*, 9245–9250.
- (21) Slinker, J. D.; Rivnay, J.; Moskowitz, J. S.; Parker, J. B.; Bernhard, S.; Abruña, H. D.; Malliaras, G. G. Electroluminescent Devices from Ionic Transition Metal Complexes. *J. Mater. Chem.* **2007**, *17*, 2976–2988.
- (22) Fernández-Hernández, J. M.; Yang, C.-H.; Beltrán, J. I.; Lemaire, V.; Polo, F.; Fröhlich, R.; Cornil, J.; De Cola, L. Control of the Mutual Arrangement of Cyclometalated Ligands in Cationic Iridium (III) Complexes. Synthesis, Spectroscopy, and Electroluminescence of the Different Isomers. *J. Am. Chem. Soc.* **2011**, *133*, 10543–10558.
- (23) Costa, R. D.; Ortí, E.; Bolink, H. J.; Monti, F.; Accorsi, G.; Armaroli, N. Luminescent Ionic Transition-Metal Complexes for Light-Emitting Electrochemical Cells. *Angew. Chem., Int. Ed.* **2012**, *51*, 8178–8211.
- (24) Baldo, M. A.; O'Brien, D. F.; You, Y.; Shoustikov, A.; Sibley, S.; Thompson, M. E.; Forrest, S. R. Highly Efficient Phosphorescent Emission from Organic Electroluminescent Devices. *Nature* **1998**, *395*, 151–154.
- (25) Adachi, C.; Baldo, M. A.; Thompson, M. E.; Forrest, S. R. Nearly 100% Internal Phosphorescence Efficiency in an Organic Light-Emitting Device. *J. Appl. Phys.* **2001**, *90*, 5048–5051.
- (26) Kwon, S.; Wee, K.-R.; Kim, J. W.; Kang, S. O. The Effect of Energy Level Offset Between Ir Dopant and Carbazole Hosts on the Emission Efficiency. *Appl. Phys. Lett.* **2010**, *97*, 023309–3.
- (27) Yarnell, J. E.; McCusker, C. E.; Leeds, A. J.; Breaux, J. M.; Castellano, F. N. Exposing the Excited-State Equilibrium in an Ir (III) Bichromophore: A Combined Time Resolved Spectroscopy and Computational Study. *Eur. J. Inorg. Chem.* **2016**, *2016*, 1808–1818.
- (28) Shao, F.; Barton, J. K. Long-Range Electron and Hole Transport Through DNA with Tethered Cyclometalated Iridium (III) Complexes. *J. Am. Chem. Soc.* **2007**, *129*, 14733–14738.
- (29) Elias, B.; Shao, F.; Barton, J. K. Charge Migration Along the DNA Duplex: Hole Versus Electron Transport. *J. Am. Chem. Soc.* **2008**, *130*, 1152–1153.
- (30) Lo, K. K.-W.; Chung, C.-K.; Zhu, N. Synthesis, Photophysical and Electrochemical Properties, and Biological Labeling Studies of Cyclometalated Iridium (III) Bis(pyridylbenzaldehyde) Complexes: Novel Luminescent Cross-Linkers for Biomolecules. *Chem. - Eur. J.* **2003**, *9*, 475–483.
- (31) Hsieh, J.-M.; Ho, M.-L.; Wu, P.-W.; Chou, P.-T.; Tsai, T.-T.; Chi, Y. Iridium-Complex Modified CdSe/ZnS Quantum Dots; A Conceptual Design for Bifunctionality Toward Imaging and Photosensitization. *Chem. Commun.* **2006**, 615–617.
- (32) Greenfield, M. T.; McGrane, S. D.; Bolme, C. A.; Bjorgaard, J. A.; Nelson, T. R.; Tretiak, S.; Scharff, R. J. Photoactive High Explosives: Linear and Nonlinear Photochemistry of Petrin Tetrazine Chloride. *J. Phys. Chem. A* **2015**, *119*, 4846–4855.
- (33) Nelson, T.; Bjorgaard, J.; Greenfield, M.; Bolme, C.; Brown, K.; McGrane, S.; Scharff, R. J.; Tretiak, S. Ultrafast Photodissociation Dynamics of Nitromethane. *J. Phys. Chem. A* **2016**, *120*, 519–526.
- (34) Ahmad, S. R.; Cartwright, M. *Laser Ignition of Energetic Materials*; John Wiley & Sons: Chichester, U.K., 2014.
- (35) Lisitsyn, V. M.; Tsipilev, V.; Damamme, G.; Malis, D. Effect of the Laser Radiation Wavelength on the Energy Threshold of Initiation of Heavy Metal Azides. *Combust., Explos. Shock Waves* **2011**, *47*, 591–600.
- (36) Renlund, A. M.; Stanton, P. L.; Trott, W. M. Laser Initiation of Secondary Explosives. In *Proceedings of the 9th International Detonation Symposium*, Portland, OR; 1989; pp 1118–1127.
- (37) Paisley, D. L. Prompt Detonation of Secondary Explosives by Laser. In *Proceedings of the 9th International Detonation Symposium*, Portland, OR; 1989; pp 1110–1117.
- (38) Joas, M.; Klapötke, T. M.; Szmhardt, N. Photosensitive Metal (II) Perchlorates with 1, 2-Bis[5-(1-methylhydrazinyl)tetrazol-1-yl]ethane as Ligand: Synthesis, Characterization and Laser Ignition. *Eur. J. Inorg. Chem.* **2014**, *2014*, 493–498.
- (39) Fischer, N.; Joas, M.; Klapötke, T. M.; Stierstorfer, J. Transition Metal Complexes of 3-Amino-1-nitroguanidine as Laser Ignitable Primary Explosives: Structures and Properties. *Inorg. Chem.* **2013**, *52*, 13791–13802.
- (40) Evers, J.; Gospodinov, I.; Joas, M.; Klapötke, T. M.; Stierstorfer, J. Cocrystallization of Photosensitive Energetic Copper (II) Perchlorate Complexes with the Nitrogen-Rich Ligand 1, 2-Di (1 H-tetrazol-5-yl)ethane. *Inorg. Chem.* **2014**, *53*, 11749–11756.
- (41) Fischer, D.; Klapötke, T. M.; Piercey, D. G.; Stierstorfer, J. Copper Salts of Halo Tetrazoles: Laser-Ignitable Primary Explosives. *J. Energ. Mater.* **2012**, *30*, 40–54.
- (42) Myers, T. W.; Bjorgaard, J. A.; Brown, K. E.; Chavez, D. E.; Hanson, S. K.; Scharff, R. J.; Tretiak, S.; Veauthier, J. M. Energetic Chromophores: Low-Energy Laser Initiation in Explosive Fe (II) Tetrazine Complexes. *J. Am. Chem. Soc.* **2016**, *138*, 4685–4692.
- (43) Myers, T. W.; Chavez, D. E.; Hanson, S. K.; Scharff, R. J.; Scott, B. L.; Veauthier, J. M.; Wu, R. Independent Control of Optical and Explosive Properties: Pyrazole-Tetrazine Complexes of First Row Transition Metals. *Inorg. Chem.* **2015**, *54*, 8077–8086.

- (44) Clavier, G.; Audebert, P. s-Tetrazines as Building Blocks for New Functional Molecules and Molecular Materials. *Chem. Rev.* **2010**, *110*, 3299–3314.
- (45) Patra, S.; Sarkar, B.; Ghumaan, S.; Patil, M. P.; Mobin, S. M.; Sunoj, R. B.; Kaim, W.; Lahiri, G. K. Isomeric Ruthenium Terpyridine Complexes $[\text{Ru}(\text{trpy})(\text{L})\text{Cl}]^{n+}$ Containing the Unsymmetrically Bidentate Acceptor $\text{L} = 3\text{-amino-6-(3, 5-dimethylpyrazol-1-yl)-1, 2, 4, 5-tetrazine}$. Synthesis, Structures, Electrochemistry, Spectroscopy and DFT Calculations. *Dalton Trans.* **2005**, 1188–1194.
- (46) Nayak, A.; Patra, S.; Sarkar, B.; Ghumaan, S.; Puranik, V. G.; Kaim, W.; Lahiri, G. K. Tetrazine Derived Mononuclear $\text{Ru}^{\text{II}}(\text{acac})_2(\text{L})$ (1), $[\text{Ru}^{\text{II}}(\text{bpy})_2(\text{L})](\text{ClO}_4)_2$ (2) and $[\text{Ru}^{\text{II}}(\text{bpy})(\text{L})_2](\text{ClO}_4)_2$ (3) ($\text{L} = 3\text{-amino-6-(3, 5-dimethylpyrazol-1-yl)-1, 2, 4, 5-tetrazine}$, $\text{acac} = \text{acetylacetonate}$, $\text{bpy} = 2, 2'\text{-bipyridine}$): Syntheses, Structures, Spectra and Redox Properties. *Polyhedron* **2005**, *24*, 333–342.
- (47) Cooper, P. W. Acceleration, Formation, and Flight of Fragments. In *Explosives Engineering*; Wiley-VCH: New York, 1996.
- (48) Chavez, D. E.; Hiskey, M. A.; Gilardi, R. D. 3, 3'-Azobis(6-amino-1, 2, 4, 5-tetrazine): A Novel High-Nitrogen Energetic Material. *Angew. Chem.* **2000**, *112*, 1861–1863.
- (49) Pagoria, P. F.; Lee, G. S.; Mitchell, A. R.; Schmidt, R. D. A Review of Energetic Materials Synthesis. *Thermochim. Acta* **2002**, *384*, 187–204.
- (50) Fried, L. E.; Manaa, M. R.; Pagoria, P. F.; Simpson, R. L. Design and Synthesis of Energetic Materials. *Annu. Rev. Mater. Res.* **2001**, *31*, 291–321.
- (51) Sabatini, J. J.; Oyler, K. D. Recent Advances in the Synthesis of High Explosive Materials. *Crystals* **2016**, *6*, 5.
- (52) Snyder, C. J.; Martin, P. D.; Heeg, M. J.; Winter, C. H. Synthesis, Structure, and Properties of Group 1 Metal Complexes Containing Nitrogen-Rich Hydrotris(tetrazolyl)borate Ligands. *Chem. - Eur. J.* **2013**, *19*, 3306–3310.
- (53) Benson, C. R.; Hui, A. K.; Parimal, K.; Cook, B. J.; Chen, C.-H.; Lord, R. L.; Flood, A. H.; Caulton, K. G. Multiplying the Electron Storage Capacity of a Bis-Tetrazine Pincer Ligand. *Dalton Trans.* **2014**, *43*, 6513–6524.
- (54) Ketterle, M.; Kaim, W.; Fiedler, J. Valence Delocalisation in a Strongly Coupled ($K_c = 10^{14}$) Molecule-Bridged Cyanodiiron (III, II) Species. *Chem. Commun.* **1998**, 1701–1702.
- (55) Bjorgaard, J. A.; Sifain, A. E.; Nelson, T. R.; Myers, T. W.; Veauthier, J. M.; Chavez, D. E.; Scharff, R. J.; Tretiak, S. Two-Photon Absorption in Conjugated Energetic Molecules. *J. Phys. Chem. A* **2016**, *120*, 4455–4464.
- (56) Casida, M. Time-Dependent Density Functional Response Theory for Molecules. In *Recent Advances in Density-Functional Methods*; Chong, D. P., Ed.; Recent Advances in Computational Chemistry; World Scientific: Singapore, 1995; Vol. 1.
- (57) Jacquemin, D.; Wathélet, V.; Perpète, E. A.; Adamo, C. Extensive TD-DFT Benchmark: Singlet-Excited States of Organic Molecules. *J. Chem. Theory Comput.* **2009**, *5*, 2420–2435.
- (58) Dreuw, A.; Head-Gordon, M. Single-Reference Ab Initio Methods for the Calculation of Excited States of Large Molecules. *Chem. Rev.* **2005**, *105*, 4009–4037.
- (59) Staroverov, V. N.; Scuseria, G. E.; Tao, J.; Perdew, J. P. Comparative Assessment of a New Nonempirical Density Functional: Molecules and Hydrogen-Bonded Complexes. *J. Chem. Phys.* **2003**, *119*, 12129–12137.
- (60) Davidson, E. R.; Feller, D. Basis Set Selection for Molecular Calculations. *Chem. Rev.* **1986**, *86*, 681–696.
- (61) Frisch, M. J.; et al. *Gaussian 09*, Revision D.02; Gaussian Inc.: Wallingford, CT, 2009.
- (62) Mennucci, B. Wiley Interdiscip. Rev.: *Comput. Mol. Sci.* **2012**, *2*, 386–404.
- (63) Scalmani, G.; Frisch, M. J.; Mennucci, B.; Tomasi, J.; Cammi, R.; Barone, V. Geometries and Properties of Excited States in the Gas Phase and in Solution: Theory and Application of a Time-Dependent Density Functional Theory Polarizable Continuum Model. *J. Chem. Phys.* **2006**, *124*, 094107.
- (64) Martin, R. L. Natural Transition Orbitals. *J. Chem. Phys.* **2003**, *118*, 4775–4777.
- (65) Jmol: An Open-Source Java Viewer for Chemical Structures in 3D. <http://www.jmol.org/> (accessed July 1, 2016).
- (66) Tao, J.; Perdew, J. P.; Staroverov, V. N.; Scuseria, G. E. Climbing the Density Functional Ladder: Nonempirical Meta-Generalized Gradient Approximation Designed for Molecules and Solids. *Phys. Rev. Lett.* **2003**, *91*, 146401.
- (67) Bühl, M.; Kabrede, H. Geometries of Transition-Metal Complexes from Density-Functional Theory. *J. Chem. Theory Comput.* **2006**, *2*, 1282–1290.
- (68) Waller, M. P.; Braun, H.; Hojdis, N.; Bühl, M. Geometries of Second-Row Transition-Metal Complexes from Density-Functional Theory. *J. Chem. Theory Comput.* **2007**, *3*, 2234–2242.
- (69) Jensen, K. P. Bioinorganic Chemistry Modeled with the TPSSH Density Functional. *Inorg. Chem.* **2008**, *47*, 10357–10365.
- (70) Zhao, Y.; Truhlar, D. G. Comparative Assessment of Density Functional Methods for 3d Transition-Metal Chemistry. *J. Chem. Phys.* **2006**, *124*, 224105.
- (71) Weymuth, T.; Couzijn, E. P.; Chen, P.; Reiher, M. New Benchmark Set of Transition-Metal Coordination Reactions for the Assessment of Density Functionals. *J. Chem. Theory Comput.* **2014**, *10*, 3092–3103.
- (72) Batista, E. R.; Martin, R. L. Natural Transition Orbitals. In *Encyclopedia of Computational Chemistry*; Wiley Online Library: Hoboken, NJ, 2004.
- (73) Reed, A. E.; Weinstock, R. B.; Weinhold, F. Natural Population Analysis. *J. Chem. Phys.* **1985**, *83*, 735–746.
- (74) Reed, A. E.; Curtiss, L. A.; Weinhold, F. Intermolecular Interactions from a Natural Bond Orbital, Donor-Acceptor Viewpoint. *Chem. Rev.* **1988**, *88*, 899–926.
- (75) Glendening, E.; Reed, A.; Carpenter, J.; Weinhold, F. *NBO, Version 3.1*; Theoretical Chemistry Institute, University of Wisconsin: Madison, WI, 1998.
- (76) Becke, A. D. Density-Functional Thermochemistry. III. The Role of Exact Exchange. *J. Chem. Phys.* **1993**, *98*, 5648–5652.
- (77) Petersson, a.; Bennett, A.; Tensfeldt, T. G.; Al-Laham, M. A.; Shirley, W. A.; Mantzaris, J. A Complete Basis Set Model Chemistry. I. The Total Energies of Closed-Shell Atoms and Hydrides of the First-Row Elements. *J. Chem. Phys.* **1988**, *89*, 2193–2218.
- (78) Petersson, G.; Al-Laham, M. A. A Complete Basis Set Model Chemistry. II. Open-Shell Systems and the Total Energies of the First-Row Atoms. *J. Chem. Phys.* **1991**, *94*, 6081–6090.
- (79) Batista, E. R.; Martin, R. L. On the Excited States Involved in the Luminescent Probe $[\text{Ru}(\text{bpy})_2\text{dppz}]^{2+}$. *J. Phys. Chem. A* **2005**, *109*, 3128–3133.
- (80) Petit, L.; Maldivi, P.; Adamo, C. Predictions of Optical Excitations in Transition-Metal Complexes with Time-Dependent Density Functional Theory: Influence of Basis Sets. *J. Chem. Theory Comput.* **2005**, *1*, 953–962.
- (81) Chardon, D. N.; McCusker, C. E.; Castellano, F. N.; Bernhard, S. Tracking of Tuning Effects in Bis-Cyclometalated Iridium Complexes: A Combined Time Resolved Infrared Spectroscopy, Electrochemical, and Computational Study. *Inorg. Chem.* **2013**, *52*, 8795–8804.
- (82) Pople, J. A.; Gill, P. M.; Johnson, B. G. Kohn—Sham Density-Functional Theory Within a Finite Basis Set. *Chem. Phys. Lett.* **1992**, *199*, 557–560.
- (83) Hay, P. J.; Wadt, W. R. Ab Initio Effective Core Potentials for Molecular Calculations. Potentials for K to Au Including the Outermost Core Orbitals. *J. Chem. Phys.* **1985**, *82*, 299–310.
- (84) Roy, L. E.; Hay, P. J.; Martin, R. L. Revised Basis Sets for the LANL Effective Core Potentials. *J. Chem. Theory Comput.* **2008**, *4*, 1029–1031.
- (85) Feller, D. The Role of Databases in Support of Computational Chemistry Calculations. *J. Comput. Chem.* **1996**, *17*, 1571–1586.
- (86) Schuchardt, K. L.; Didier, B. T.; Elsethagen, T.; Sun, L.; Gurumoorthi, V.; Chase, J.; Li, J.; Windus, T. L. Basis Set Exchange: A

Community Database for Computational Sciences. *J. Chem. Inf. Model.* **2007**, *47*, 1045–1052.

(87) Masunov, A.; Tretiak, S. Prediction of Two-Photon Absorption Properties for Organic Chromophores using Time-Dependent Density-Functional Theory. *J. Phys. Chem. B* **2004**, *108*, 899–907.

(88) Bowman, D. N.; Bondarev, A.; Mukherjee, S.; Jakubikova, E. Tuning the Electronic Structure of Fe (II) Polypyridines via Donor Atom and Ligand Scaffold Modifications: A Computational Study. *Inorg. Chem.* **2015**, *54*, 8786–8793.

(89) Gray, C.; Gubbins, K. *Theory of Molecular Fluids, Volume 1: Fundamentals*; Oxford University Press: Oxford, U.K., 1984.

(90) Agrawal, J. P. *High Energy Materials: Propellants, Explosives and Pyrotechnics*; Wiley-VCH: Weinheim, Germany, 2010.

(91) Kalyanasundaram, K. Photophysics, Photochemistry and Solar Energy Conversion with Tris(bipyridyl)ruthenium(II) and its Analogues. *Coord. Chem. Rev.* **1982**, *46*, 159–244.

(92) Braterman, P. S.; Song, J. L.; Peacock, R. D. Electronic Absorption Spectra of the Iron (II) Complexes of 2, 2'-bipyridine, 2, 2'-bipyrimidine, 1, 10-phenanthroline, and 2, 2': 6', 2''-terpyridine and Their Reduction Products. *Inorg. Chem.* **1992**, *31*, 555–559.

(93) Tsipis, A. C. DFT Flavor of Coordination Chemistry. *Coord. Chem. Rev.* **2014**, *272*, 1–29.